Numerical Simulation of Gas and Liquid Two-Phase Flow in Gas-Stirred Systems Based on Euler–Euler Approach

WENTAO LOU and MIAOYONG ZHU

Based on the Euler–Euler approach, a mathematical model is established to describe gas and liquid two-phase flow in the gas-stirred system for steelmaking, and the influences of the interphase force including turbulent dispersion force, drag force, and lift force are investigated. The modified k–ε model with extra source terms to account for the bubble-induced turbulence is adopted to model the turbulence in the system, and the simulation results of gas volume fraction, liquid velocity, and turbulent kinetic energy are compared with the measured data. The results show that the turbulent dispersion force dominates the bubbly plume shape and is responsible for successful prediction of the gas volume fraction. The bubble-induced turbulence has a significant influence on the liquid turbulence, and the conversion coefficient C_b, which denotes the fraction of bubble-induced energy converted into liquid turbulence, should be in the range of 0.8 and 0.9. The drag force also strongly influences the bubbly plume dynamics, and the coefficient model proposed by Kolev performs the best for determining the drag force; however, the lift force and bubble diameter do not have much effect on the current bubbly plume system. For different gas flow rates, the current Euler–Euler approach predictions are more consistent with the measured data than the Euler–Lagrange approach and the early Euler–Euler model.

I. INTRODUCTION

THE gas-stirred system is of enormous importance in steelmaking process, and bubbly plume flow is produced by the blowing of inert gas through the ladle bottom (Figure 1), which usually is used to promote stirring of melt and chemical reactions, to enhance inclusion removal, and to homogenize the temperature and composition of the melt. In some cases, it can also be treated as transport carrier to injection powder, such as desulfurization powder and alloy powder. Because the most intensive mass and heat transfer occur in the bubbly plume region, it is vital to acquire more knowledge of the plume behavior in the gas-stirred system.

Currently, there is a quasi-single-phase model[1–10] and a two-phase model[11–22] to describe the gas–liquid two-phase flow in a gas-stirred ladle, and the two-phase model can be divided into the Euler–Lagrange approach[11–15] and Euler–Euler approach,[16–23] depending on how the dispersed phase is treated. These models have their own advantages and disadvantages.

In quasi-single-phase model, the gas–liquid mixture phase is modeled as a homogeneous fluid with reduced density such as $\rho = \alpha \rho_g + (1 - \alpha_g) \rho_1$, where α_g is the gas volume fraction, and this model is computationally more economical than the two-phase model. However, because the interaction forces between gas and liquid two-phase, such as drag force, lift force, etc., are neglected in the model, the velocity and turbulent kinetic energy could not be described properly in the bubbly plume region. Furthermore, it has been also recognized that the gas volume fraction distribution in the ladle needs to be prespecified and usually obtained from empirical correlations, so the application of the model is limited.

In the Euler–Lagrange approach, the mass and momentum conservation equations are solved only for liquid phase under an Eulerian reference frame, and the discrete phase is treated as individual particles and their trajectories are described by integrating the force balance on particle under a Lagrangian reference frame. In this approach, the interphase forces are taken into account through the momentum source term, and the simulation results agree well with measured results under a low gas flow rate. However, the application of the Euler–Lagrange approach assumes that the particle volume fraction is generally not more than 12 pct,[24] and the impact among particles is ignored. The coordinate system is different between discrete phase and continuous phase, and the discrete phase does not occupy any space continuous volume under the Eulerian coordinate system, so the effect of the volume fraction of the discrete phase on the continuous phase is neglected. To solve this problem, Sheng and Irons[12,13] and Guo and Irons[14] calculated the time-averaged bubble volume fraction by statistics of number and residence time of discrete particles in grid control cell as Eq. [1],

$$\alpha_g = \frac{1}{T V_{\text{cell}}} \sum_{i=1}^{N} V_{\text{bub},pi} dt_i \qquad [1]$$

WENTAO LOU, Ph.D. Candidate, and MIAOYONG ZHU, Professor, are with the School of Materials and Metallurgy, Northeastern University, Shenyang 110819, P.R. China. Contact e-mail: myzhu@mail.neu.edu.cn
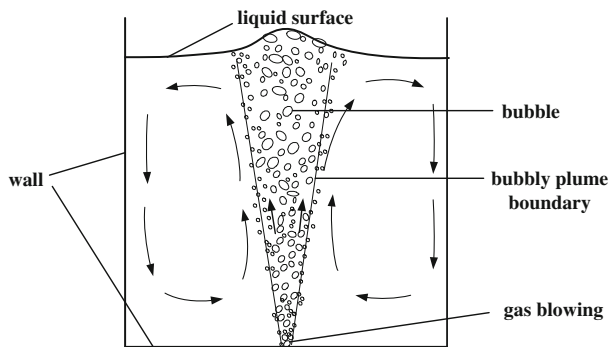
Fig. 1—Characteristics of bubbly plume flow in gas-stirred systems.

where V_{cell} is the grid cell volume, N is number of bubbles particle released from the gas inlet, and $V_{bub,pi}$, dt_i are the volume and residence time of the ith bubble in the control cell volume, respectively. Even so, the time-averaged gas volume fraction is still affected by grid size and the particle number released from the gas inlet, and the particle stochastic trajectory will also increase the instability of spatial distribution of the gas volume fraction.

In the Euler–Euler approach, both phases are treated as interpenetrating fluids, and the laws of conservation of mass and momentum are satisfied by each phase individually. Thus, the above mentioned difficulties do not arise with the Euler–Euler approach. However, compared with experimental results, the predicted results of bubbly plume system using Euler–Euler approach are still unsatisfactory. Several publications[22,23] employed the Euler–Euler approach to describe the bubbly plume, but the shape of the rising plume appeared with flat distribution and the width of the plume was essentially the same along the vertical direction, which is obviously inconsistent with the experimental results. Ilegbusi *et al.*[18–20] used the liquid turbulent viscosity to represent the turbulent diffusion of phase mass, and the predicted gas volume fraction was close to the measured data. However, the predicted liquid velocity and turbulence were still not consistent with the measured results.

For the Euler–Euler model, the main factors that affect accurate predictions of gas–liquid two-phase flow are as follows:

(a) Bubbles turbulent dispersion due to the liquid velocity fluctuation. In the Euler–Euler approach, the turbulent dispersion of particles is neglected due to the averaging procedure for flow field. So, the turbulent diffusion effects must be added in the form of source terms of conservation equations. Ilegbusi *et al.*[18–20] used the liquid turbulent viscosity included in the source term of mass conservation equation to represent the bubble diffusion by assuming the phase mass diffusion similar to species transport. On the other hand, some researchers[25–32] considered the bubble diffusion due to extra interphase force and proposed the concepts called

"turbulent diffusion force" to describe the particle turbulent diffusion, which was included in the source term of momentum conservation equation. Mudde and Simonin[32] applied this method for simulations of a bubbly plume based on the Euler–Euler approach, but the bubble-induced turbulence was not considered.

(b) Interphase force. Unfortunately, there have not been unified expressions for the drag force, lift, virtual mass force, *etc.*, and the different drag force coefficient models[33–40] and the lift force coefficient[41–45] were adopted in the previous studies. Selecting the appropriate interfacial force model is very important for correctly predicting the gas and liquid two-phase flow.

(c) Bubble-induced turbulence. Due to velocity slip between the gas–liquid two phases, the additional liquid turbulent kinetic energy is produced during the bubble-rising process. But in different gas-stirred systems, C_b, which denotes the fraction of bubble-induced energy converted into liquid turbulent kinetic energy, had a different description.[46–48] Selecting the appropriate C_b value is the basis for correctly predicting the turbulence of bubbly plume.

The objectives of the current work are to present a mathematical model to describe the gas-stirred system for steelmaking based on the Euler–Euler approach, as well as to predict the gas volume fraction distribution and the bubble-induced turbulence more reasonably. Therefore, the effects of the bubble turbulent dispersion, bubble-induced turbulence, and interphase force, such as drag force and lift force on the bubbly plume, are investigated, and the simulation results of gas volume fraction, liquid velocity, and turbulent kinetic energy are compared with the measured data. By assessing the current model, the Euler–Lagrange approach, and the early Euler–Euler model, some new comments for accurately describing the bubbly plume flow in a gas-stirred system for steelmaking with Euler–Euler approach are given.

II. GOVERNING EQUATIONS FOR TWO-PHASE FLUID

The flow is assumed to be isothermal and at the steady state, and the energy balance and chemical reactions are not involved. The liquid density is uniform constant, the bubble density ρ_g is treated as a function of liquid static pressure P, and an ideal gas law is used.

$$\rho_g = P M_{Wg}/(RT) \qquad [2]$$

$$P = P_{op} + \bar{g}\rho_l(H - z) \qquad [3]$$

where R is the universal gas constant, M_{Wg} is the molecular weight of gas phase, P_{op} is the operating pressure, H is the bath liquid height, and z is the height from the bath bottom.

Table I. Five Different Models for the Drag Coefficient C_D

Model	Correlation	Reference
A	$C_D = \begin{cases} 24/\mathrm{Re}(1+0.15\mathrm{Re}^{0.687}), & \text{if } \mathrm{Re} < 1000 \\ 0.44, & \text{if } \mathrm{Re} \geq 1000 \end{cases}$	Delnoij et al.[33] Djebbar et al.[34]
B	$C_D = \mathrm{Max}\left[\mathrm{Min}\left[\frac{24}{\mathrm{Re}}\left(1+0.15\mathrm{Re}^{0.687}\right), \frac{72}{\mathrm{Re}}\right], \frac{8}{3}\frac{Eo}{(Eo+4)}\right]$	Tomiyama et al.[35,36]
C	$C_D = \frac{2}{3}Eo^{0.5}$	Ishii and Zuber[37]
D	$C_D = \begin{cases} 24/\mathrm{Re} & \text{if } \mathrm{Re} < 0.49 \\ 20.68/\mathrm{Re}^{0.643} & \text{if } 0.49 < \mathrm{Re} < 100 \\ 6.3/\mathrm{Re}^{0.385} & \text{if } \mathrm{Re} > 100,\ We \leq 8 \text{ and } \mathrm{Re} \leq 2065.1/We^{2.6} \\ We/3 & \text{if } \mathrm{Re} > 100,\ We \leq 8 \text{ and } \mathrm{Re} > 2065.1/We^{2.6} \\ 3/8 & \text{if } \mathrm{Re} > 100,\ We > 8 \end{cases}$	Kuo and Wallis[38] Boisson and Malin[39]
E	$\begin{cases} C_{Dvis} = 24/\mathrm{Re}\left(1+0.1\mathrm{Re}^{0.75}\right) & \text{if } C_{Ddis} < C_{Dvis},\ C_D = C_{Dvis} \\ C_{Ddis} = 2/3\left(\frac{(\bar{g}\rho_1)^{0.5}d_g}{\sigma^{0.5}}\right)\left(\frac{1+17.67(1-\alpha_g)^{1.286}}{18.67(1-\alpha_g)^{1.5}}\right)^2 & \text{if } C_{Dvis} < C_{Ddis} < C_{Dcap},\ C_D = C_{Dvis} \\ C_{Dcap} = 3/8\left(1-\alpha_g\right)^2 & \text{if } C_{Ddis} > C_{Dcap},\ C_D = C_{Dcap} \end{cases}$	Kolev[40]

A. Eulerian Multiphase Hydrodynamic Equations

Based on the Euler–Euler approach, the mass and momentum balance equations are used for each phase separately. The interaction forces between the gas and liquid phases are considered as momentum exchange source terms in the momentum equations.

Mass conservation:

$$\nabla \cdot (\alpha_k \rho_k \bar{u}_k) = 0 \qquad [4]$$

where, ρ_k, α_k, and $\bar{u}_k$, are the density, volume fraction, and phase-averaged velocity of liquid phase ($k = l$) and the gas phase ($k = g$), respectively.

Momentum conservation:

$$\nabla \cdot (\alpha_k \rho_k \bar{u}_k \bar{u}_k) = -\alpha_k \nabla p + \nabla \cdot \left(\alpha_k \mu_{\mathrm{eff}}\left(\nabla \bar{u}_k + (\nabla \bar{u}_k)^T\right)\right) \\ + \alpha_k \rho_k \bar{g} + \overline{M}_k \qquad [5]$$

$$\mu_{\mathrm{eff}} = \mu_l + \mu_t \qquad [6]$$

$$\mu_t = C_\mu \rho_l \frac{k_l^2}{\varepsilon_l} \qquad [7]$$

where $\bar{g}$ is the acceleration due to gravity; and μ_l, μ_t, and μ_{eff} are the liquid molecular viscosity, turbulent viscosity, and effective viscosity, respectively; p is the pressure, which is shared by both the phases; and $\overline{M}_k$ is the interfacial momentum exchange term between the gas and liquid.

B. Interphase Forces $\overline{M}_k$

From Eq. [5], it is noted that closure law is required to determine the momentum transfer of the interphase force $\overline{M}_k$, which is described as follows:

$$\overline{M}_l = -\overline{M}_g = F_D + F_{VM} + F_L + F_{TD} \qquad [8]$$

where the terms on the right-hand side represent force due to drag, virtual mass, lift, and turbulent dispersion force, respectively. Here, $\overline{M}_l(\overline{M}_g)$ denotes the momentum transfer terms from the gas (liquid) phase to liquid (gas) phase.

1. Drag force F_D

The drag force is the dominant contribution to the interaction force. It is common to describe the drag force F_D as follows:

$$F_D = K_{gl}(\bar{u}_g - \bar{u}_l) \qquad [9]$$

$$K_{gl} = \frac{3\alpha_g \alpha_l \rho_l C_D}{4d_g}|\bar{u}_g - \bar{u}_l| \qquad [10]$$

where, K_{gl} is the interphase momentum exchange coefficient due to drag force and d_g is the diameter of the bubbles. According to the study of Sano and Mori,[49] the bubble diameter is calculated as follows:

$$d_g = \left[\left(\frac{6\sigma d_0}{\rho_l g}\right)^2 + 0.0248\left(Q_g^2 d_0\right)^{0.867}\right]^{\frac{1}{6}} \qquad [11]$$

where, Q_g is the gas flow rate, d_0 is the nozzle diameter, and σ is the gas–liquid surface tension coefficient.

In Eq. [10], C_D is the drag force coefficient, and the different correlations for C_D are presented in Table I. In the current model, the numerical results with these different drag coefficients models would be compared with the measured data, and the reasonable drag force coefficient would be determined, which will be discussed later.

2. Lift force F_L

The lift force mainly includes the Saffman force due to the shear in the mean flow and the Magnus force resulting from the asymmetric pressure distribution because of a particle rotation. The bubbly plume flow is so complex that no accurate theoretical model for the lift force is available in the literature. For the simulation of bubbly plume flow, the lift force is calculated from the following expression:

$$F_L = -\alpha_g C_L \rho_l (\bar{u}_g - \bar{u}_l) \times (\nabla \times \bar{u}_l) \qquad [12]$$

where C_L is the lift force coefficient, which is different among the literature. Some authors[33,41,42] adopted a value of 0.5, but Lopez de Bertodano et al.[43] suggested the value between 0.02 and 0.1. There are also some References 37, 38, 46 that show the life coefficient is defined as negative values. For the current bubbly plume flow, the lift coefficient was determined by comparing the numerical results with measured data.

3. Virtual mass force F_{VM}

If the bubbles accelerate relative to the liquid, then part of the surrounding liquid has to be accelerated as well, and the additional force contribution is called as virtual mass force F_{VM}, which can be calculated by:

$$F_{VM} = C_A \alpha_g \rho_l \cdot \left(\frac{d\bar{u}_g}{dt} - \frac{d\bar{u}_l}{dt} \right) \qquad [13]$$

where C_A is the virtual mass force coefficient. But in a gas-stirred system, the influence of the virtual mass on the measurement and simulation results was found to be extremely weak.[50] The virtual mass force can be safely neglected is based on the premise that the gas bubble velocity gradient is very small. In the current water model ladle, the large bubble velocity gradient only appears in a short distance from the bottom blowing device, and this distance relative to the whole water model ladle can be ignored. Therefore, the virtual mass force is neglected in the current model.

4. Turbulent dispersion force F_{TD}

Based on the Tchen theory, some researchers[27–31] proposed the concept of the drift velocity to express the effect of fluid turbulent fluctuation on the particle dispersion, and the turbulent dispersion force can be written as follows:

$$F_{TD} = -K_{gl} u_{drift} \qquad [14]$$

$$u_{drift} = \frac{D_{gl}^t}{\omega_{gl}} \left(\frac{1}{\alpha_l} \nabla \alpha_l - \frac{1}{\alpha_g} \nabla \alpha_g \right) \qquad [15]$$

where the u_{drift} is the drift velocity, which represents the correlation between the liquid fluctuating velocity and the spatial distribution of the particles, ω_{gl}, a dispersion Prandtl number, can be set 0.75, and D_{gl}^t, the turbulent dispersion coefficient, can be expressed as:

$$D_{gl}^t = \frac{1}{3} k_{gl} \tau_{gl}^t \qquad [16]$$

where k_{gl} is the covariance coefficient between the turbulent velocity fluctuations of the two phases, and τ_{gl}^t is a fluid bubble turbulent characteristic time.

$$k_{gl} = 2k_l \left[\frac{b + \eta_r}{1 + \eta_r} \right] \qquad [17]$$

$$\eta_r = \frac{\tau_{gl}^t}{\tau_{gl}^F} \qquad [18]$$

$$\tau_{gl}^t = \frac{\tau_l^t}{\omega_{gl}} [1 + C_\beta \zeta^2]^{-0.5} \qquad [19]$$

$$\tau_{gl}^F = \frac{1}{K_{gl}} \alpha_g \rho_l \left(\frac{\rho_g}{\rho_l} + C_A \right) \qquad [20]$$

$$\tau_l^t = \frac{3}{2} C_\mu \frac{k_q}{\varepsilon_q} \qquad [21]$$

where τ_{gl}^F is the characteristic time of particle entrainment by the continuous fluid motion, and τ_l^t is the characteristic time of the energetic turbulent eddies.

$$\zeta = \frac{|\bar{u}_g - \bar{u}_l|}{\sqrt{(2/3)k_l}} \qquad [22]$$

$$C_\beta = 1.8 - 1.35 \cos^2 \theta \qquad [23]$$

$$b = (1 + C_A) \left(\frac{\rho_p}{\rho_q} + C_A \right)^{-1} \qquad [24]$$

where θ is the angle between the mean particle velocity and the mean relative velocity.

C. Turbulence Models

The k–ε model is originally used to solve the single-phase turbulence, and for the gas and liquid two-phase flow, turbulence modeling such as bubble-induced turbulence and interaction source terms between two phases turbulence are still the main unresolved problems.

To account for the additional turbulent kinetic energy produced by the bubble motion, the bubble-induced turbulence is generally accounted for by source terms appearing in the equations of k–ε.

$$\frac{\partial}{\partial t}(\alpha_l \rho_l k_l) + \nabla \cdot (\alpha_l \rho_l \bar{u}_l k_l) = \nabla \cdot \left(\alpha_l \frac{\mu_t}{\sigma_k} \nabla k_l \right)$$
$$+ \alpha_l G_{k,l} + \alpha_l G_b - \alpha_l \rho_l \varepsilon_l + \alpha_l \rho_l \Pi_{k,l} \qquad [25]$$

$$\frac{\partial}{\partial t}(\alpha_l \rho_l \varepsilon_l) + \nabla \cdot (\alpha_l \rho_l \bar{u}_l \varepsilon_l) = \nabla \cdot \left(\alpha_l \frac{\mu_t}{\sigma_\varepsilon} \nabla \varepsilon_l \right)$$
$$+ \alpha_l \frac{\varepsilon_l}{k_l} \left(C_{1\varepsilon}(G_{k,l} + G_b) - C_{2\varepsilon} \rho_l \varepsilon_l \right) + \alpha_l \rho_l \Pi_{\varepsilon,l} \qquad [26]$$

Table II. Model Constants Employed in Turbulent Model

C_μ	$C_{1\varepsilon}$	$C_{2\varepsilon}$	$C_{3\varepsilon}$	σ_k	σ_ε	ω_{gl}
0.09	1.44	1.92	1.2	1.0	1.3	0.75

where k_l, ε_l are the turbulent kinetic energy and the dissipation rate of the continuous phase, respectively, and σ_k, σ_ε, $C_{1\varepsilon}$, $C_{2\varepsilon}$ are model constants summarized in Table II; $G_{k,l}$ denotes the production of turbulence kinetic energy due to the liquid phase mean velocity gradients; and G_b is the additional bubble-induced turbulent kinetic energy.

$$e_R = (\rho_l - \rho_g) g \alpha_g \bar{u}_g \qquad [27]$$

$$e_D = (\rho_l - \rho_g) g \alpha_g (\bar{u}_g - \bar{u}_l) \qquad [28]$$

In a turbulent rising bubble plume, e_R is the total rate of pressure energy lost by the bubble, and e_D is the rate of the energy converted into turbulence and spent in the viscous dissipation, which depends only on the slip velocity.[51]

$$G_b = C_b e_D \qquad [29]$$

where C_b ($0 < C_b < 1$) denotes the fraction of bubble-induced energy converted into the liquid phase turbulence. Lopez de Bertodano *et al.*[52] adopted the C_b value of 0.02 for low gas fractions, and at higher gas fractions, a value of C_b ranging between 0.1 and 0.7 was suggested by Johansen and Boysan.[11] But there are still no detailed traffic data to develop the relationship between C_b and the gas flow rate. In this article, to reduce the sensitivity of C_b value to the gas flow rate, Eq. [29] is modified as follows:

$$G_b = C_b \frac{\mu_t}{\mu_{eff}} (\rho_l - \rho_g) g \alpha_g \bar{u}_{rel} \qquad [30]$$

$\Pi_{k,l}$, $\Pi_{\varepsilon,l}$,[53,54] in Eqs. [25] and [26], represent the influence of the dispersed phases turbulence on the continuous phase turbulence, which can be expressed as

$$\Pi_{k,l} = K_{gl} \frac{\rho_g}{\rho_l + \rho_l C_A} \left(-2k_l + k_{gl} + \bar{u}_{rel} \cdot \bar{u}_{drift} \right) \qquad [31]$$

$$\Pi_{\varepsilon,l} = C_{3\varepsilon} \frac{\varepsilon_l}{k_l} \Pi_{k,l} \qquad [32]$$

III. BOUNDARY CONDITIONS

In this work, the commercial computational fluid dynamics software Fluent 12.0 combined with user-defined function (UDF) (Ansys Inc., Canonsburg, PA) was used to simulate gas and liquid two-phase flow in the bottom blowing ladle. The dimensions of water model ladle and other parameters employed in the current model are shown in Table III. Figure 2 shows

Table III. The Dimensions of Water Model Ladle and Other Parameters Employed in Model

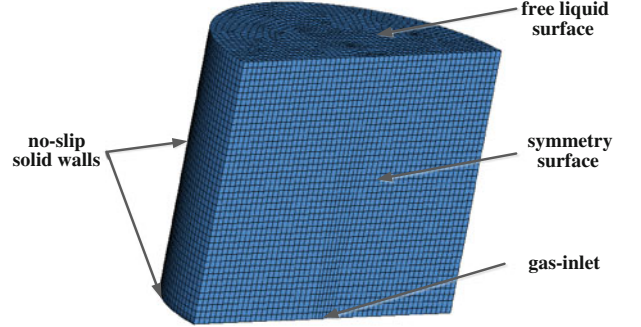|	
Diameter of water model ladle	500 mm
Bath depth	420 mm[12]
	400 mm[55]
Orifice diameter	4 mm[12]
	6.35 mm[55]
Gas flow rates	50 and 150 mL/s[12]
	371 mL/s[55]
Density of water	1000 kg/m^3
Density of gas	1.225 kg/m^3
Molecular viscosity of water	0.001 Pa s
Surface tension between water and gas	0.073 N/m

Fig. 2—Mesh and boundary conditions of water model ladle.

the mesh and boundary conditions of the water model ladle, and due to the symmetry of the flow, only half of the geometric model is built as a computational domain. The boundary conditions are set based on the experimental conditions used by Castillejos and Brimacombe[55] and Sheng and Irons.[12] The bottom and side walls were set as no-slip solid walls, and the standard wall function was used to model the turbulence characteristic in the near-wall region. The velocity-inlet was used for gas blowing at the bottom tuyeres, and a free liquid surface was assumed at the top surface, where there is an outlet for the gas and a free slip wall for the liquid. The bubble diameter is treated as a constant and is calculated with the Eq. [11].

IV. RESULTS AND DISCUSSION

A. *The Effect of Turbulent Dispersion Force*

Figure 3 shows the effect of turbulent dispersion force on the gas volume fraction distribution. The diameters of water model and bottom nozzle are 500 mm and 4 mm, respectively, and the liquid height is 420 mm. It can be seen from the figure that the turbulent dispersion force dominates the bubble plume shape. When the turbulent dispersion force is not considered in the current model, the effect of liquid turbulent fluctuation velocity on the bubble dispersion is neglected due to the averaging procedure for flow field in the Euler–Euler approach, and the size of the bubbly plume is relatively narrow and almost keeps the same width along the

vertical direction. Conversely, when the turbulent dispersion is considered, the bubbly plume produces dispersion due to the liquid velocity fluctuation during the bubble rising, and the plume centerline gas volume fraction decreases with the height increasing far from the bath bottom.

Figure 4 presents the comparison between the predicted results with turbulent dispersion force considered in Euler–Euler approach and the measured data[55] in the water model. The internal diameters of water model and bottom nozzle are 500 mm and 6.35 mm, respectively; the liquid height is 400 mm; and the gas flow rate is 371 mL/s. From the figure, it can be seen that the predicted bubbly plume shape and gas volume fraction agree very well with the measured results, and the turbulent dispersion force is responsible for successful prediction of the gas volume fraction.

B. The Effect of Bubble Induced Turbulence

Figures 5 and 6 show the effect of bubble-induced turbulence on liquid velocity and turbulent kinetic energy, respectively. It should be noted that the liquid velocity in bubbly plume region becomes lower, and the liquid turbulent kinetic energy becomes greater than the case without G_b considered in model. This is because that in gas-stirred turbulent flow, the total energy e_R (Eq. [27]) generated during bubble rising, is converted into liquid internal energy e_D (Eq. [28]) due to slip velocity and liquid kinetic energy ($e_R - e_D$). When the bubble-induced turbulent G_b is considered in the current model, a portion of the total energy e_R would be first converted into liquid turbulent kinetic energy and then finally into internal energy e_D due to turbulent dissipation rate. Therefore, subsequently the energy converted into liquid kinetic energy ($e_R - e_D$) is reduced, and the liquid velocity driven by bubble would become lower. Furthermore, it can be seen from Figure 4 that the maximum turbulent kinetic energy appears near bottom tuyeres, and compared with the turbulent kinetic energy generated by the liquid mean velocity gradients, the

bubble-induced turbulence has significant influence on the liquid turbulence and could not be ignored in modeling.

Figure 7 shows the effect of different turbulence conversion coefficient C_b on the liquid axial velocity and turbulent kinetic energy along the plume centerline, and a comparison of predicted results with measured data of Sheng and Irons.[12] It is clear that with C_b increasing, the more energy generated during the bubbles rising is converted into liquid turbulent kinetic energy, and subsequently, the remaining energy converted into liquid kinetic energy is reduced, so the liquid velocity driven by bubble would become lower. When the C_b ranges between 0.8 and 0.9, the predicted liquid velocity and turbulent kinetic energy agree well with the measured, and the value of C_b is uniformly taken as 0.85 in the current work.

C. The Effect of Drag Force Coefficient

In the current model, different drag coefficient models, as shown in Table I, are adopted to describe the bubbly plume system, and all the model parameters are not changed except for the drag force coefficient closure model. Figure 8 provides the effect of different drag force coefficient on the liquid axial velocity and turbulent kinetic energy along the plume centerline, and the predicted results are compared with the measured data.[12] It is found that the drag coefficient strongly influences the bubbly plume dynamics, and the predicted result agrees well with the measured as the drag coefficient model proposed by Kolev[38] (model F in Table I) is adopted. When the drag coefficient of model A (Table I) is adopted in the model, the drag force between gas and liquid is underestimated, and the lesser portion of total energy generated during the bubbles rising is converted into liquid kinetic energy. Subsequently, the greater portion would be converted into turbulent kinetic energy. Therefore, the liquid velocity is underpredicted, while the liquid turbulent energy was overpredicted. Conversely, when the drag coefficient of
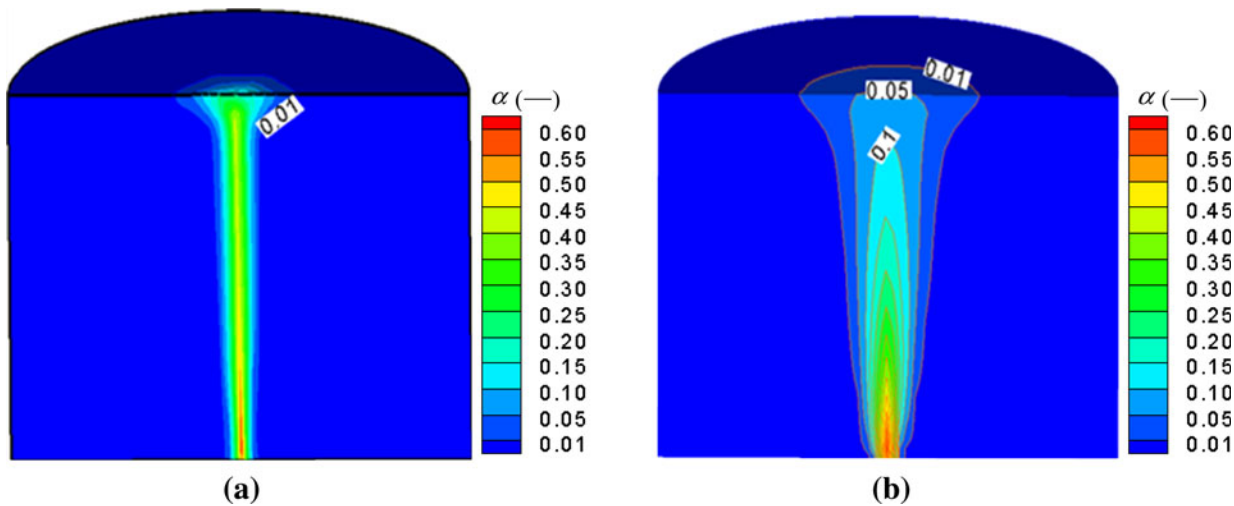

Fig. 3—Effect of turbulent dispersion force F_{TD} on the gas volume fraction distribution: (a) without F_{TD} and (b) with F_{TD}.

models B, C, and D in Table I are adopted in the model, the liquid velocity is overpredicted, while the liquid turbulent kinetic energy are underpredicted.

D. *The Effect of Lift Force Coefficient*

To determine the appropriate lift force coefficient for ladle, in the current model, the numerical prediction with different lift coefficient from 0.5 to −0.05 are compared with the experimental data.

Figure 9 provides a comparison of the predicted contours map of the gas volume fraction with different lift coefficient. From this figure, it can be observed that when the lift coefficient decreases from 0.5 to −0.05, the gas phase is gradually gathered to the center and the bubbly plume shape become narrower. This is because the lift force acting on the bubbles is mainly on the radial, which put the bubbles away from the plume

central with a positive lift coefficient, and it gathers the bubbles to the center with a negative lift coefficient.

Figure 10 shows the effect of different lift coefficient on the liquid axial velocity and turbulent kinetic energy, as well as a comparison of the predicted results with the measured data[12] along the plume centerline. It is noticed that the liquid velocity and turbulent kinetic energy increase with the lift force coefficient decreasing from 0.5 to −0.05, and when the lift coefficient C_L ranges between 0.01 and −0.01, the predicted liquid velocity and turbulent kinetic energy agree well with the measured data. Clearly, the lift force has a small influence on the current bubble plume flow system.

E. *The Effect of Bubble Diameter*

In the current gas-stirred system, the bubble diameter is treated as a constant and calculated with Eq. [11].
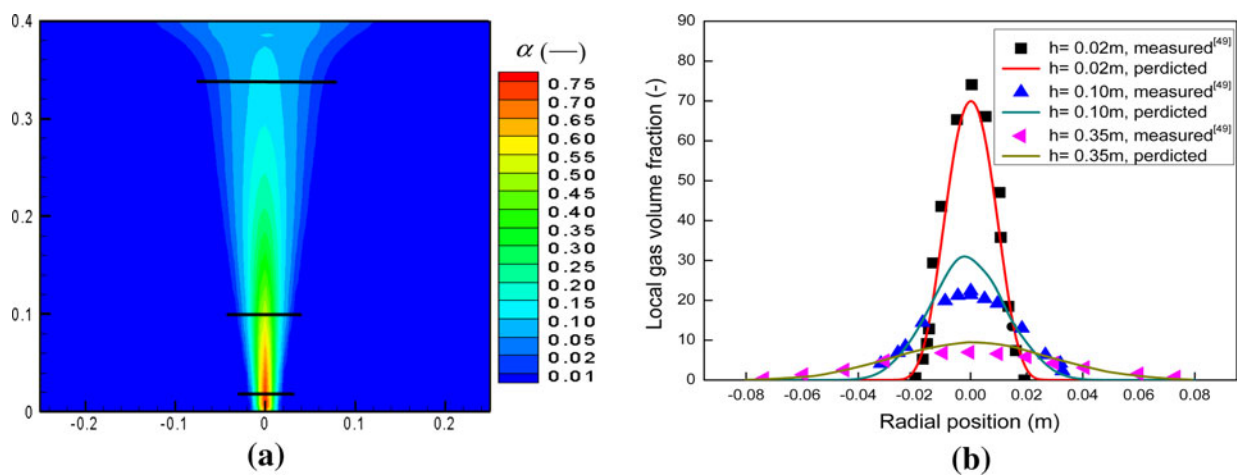

Fig. 4—(*a*) Predicted contour map of gas volume fraction under the same experimental conditions as referenced by Castillejos and Brimacombe.[55] (*b*) Comparison of predicted and measured local gas fraction along the radial direction at heights of 0.02 m, 0.10 m, and 0.35 m.
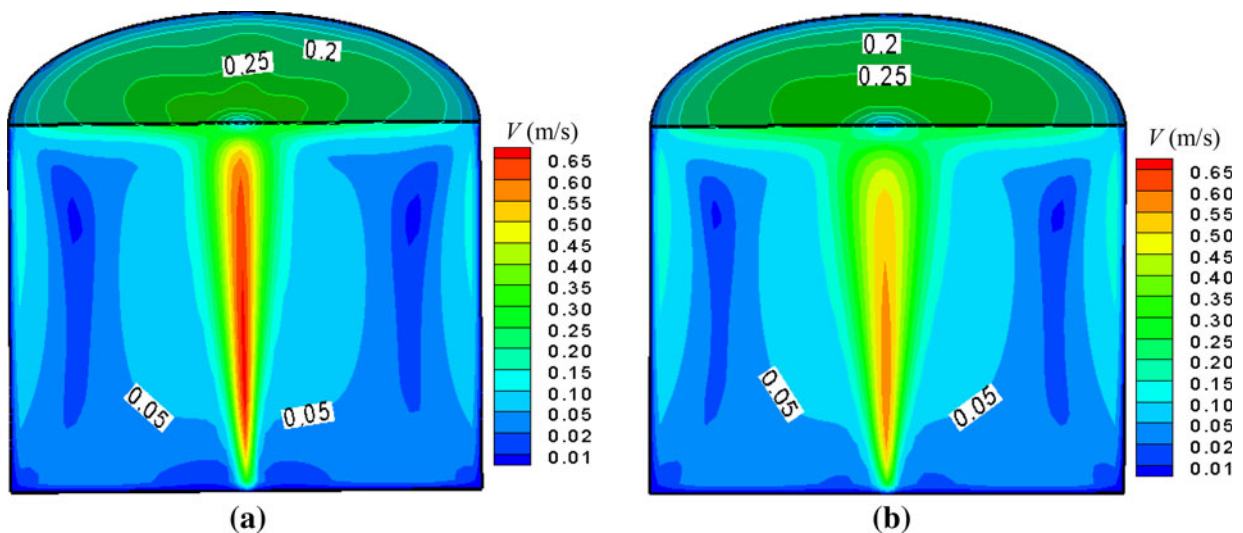

Fig. 5—Effect of bubble-induced turbulence G_b on the contours of liquid velocity V (m/s): (*a*) without G_b and (*b*) with G_b.
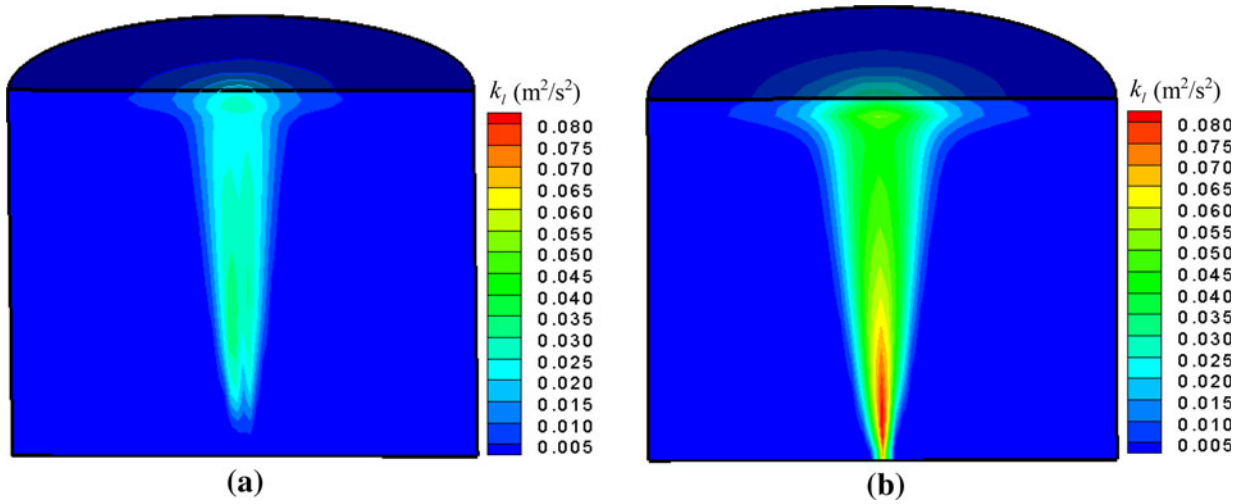
Fig. 6—Effect of bubble-induced turbulence G_b on the contours of liquid turbulent kinetic energy k_l (m^2/s^2): (a) without G_b and (b) with G_b.
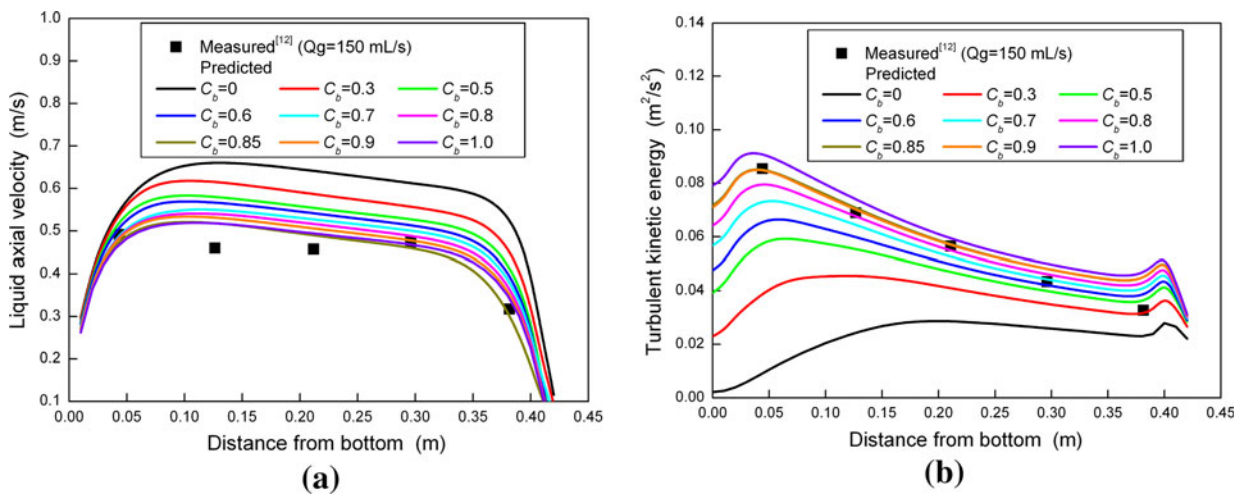

Fig. 7—Comparison between predicted results with different turbulent conversion coefficient G_b and measured data by Sheng and Irons[12] along the plume centerline: (a) liquid axial velocity and (b) turbulent kinetic energy.
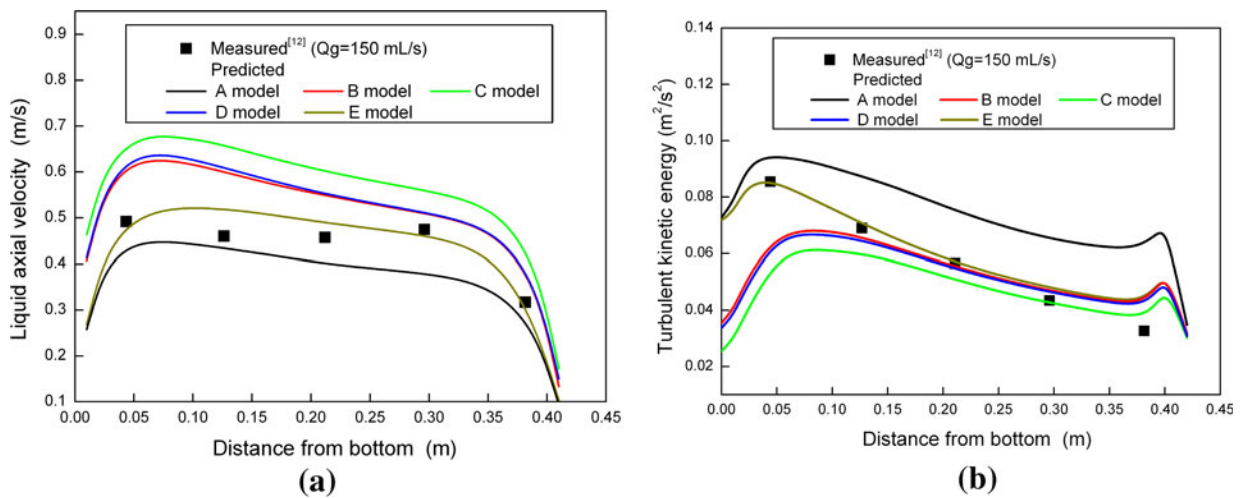

Fig. 8—Comparison between predicted results with different drag coefficient C_D and measured data by Sheng and Irons[12] along the plume centerline: (a) liquid axial velocity and (b) turbulent kinetic energy.

However, in fact, the bubbles size is variable because the bubbles coalescence and breakup in the plume zone. Therefore, the effect of the bubble diameter on the bubbly plume flow needs to be investigated. In the current model, different bubbles diameter from 13 mm to 25 mm are adopted to predict the bubbly plume system, and all the model parameters were not changed except for the bubble diameter.

Figure 11 provides the effect of different bubble diameter on the liquid axial velocity and turbulent kinetic energy along the plume centerline. From this figure, it can be found that with the increase of bubble diameter from 13 mm to 25 mm, the liquid velocity decreases slowly, while the liquid turbulent kinetic energy increases slowly. This is because that as the bubble diameter increased, the slip velocity between bubble and liquid would become greater, and the more bubble induced turbulence G_b would be generated. But overall, the changes of bubble diameter within the small range have a weak impact on the current bubbly plume.

F. *The Applicability of the Model*

The model parameters for describing the turbulent behavior in gas-stirred system have been determined based on their sensitivity study, and the applicability of the model still needs to be verified further. Figures 12 through 14 compare the predicted gas volume fraction, liquid velocity, and turbulent kinetic energy using various models with the measured data, and the performances of the current model, the Euler–Lagrange model proposed by Sheng and Irons,[12–14] and the early Euler–Euler model proposed by Ilegbusi et al.[18–20] were assessed. In the current work, the comparison results predicted by the current model and the early Euler–Euler model are based on the same grid to avoid numerical artifact.

Figure 12 shows the contour map of gas volume fraction predicted by the current Euler-Euler approach with previously determined parameters and compares the predicted results of three different models with measured data.[12] It is found from the figure that the current model predictions are more consistent with the
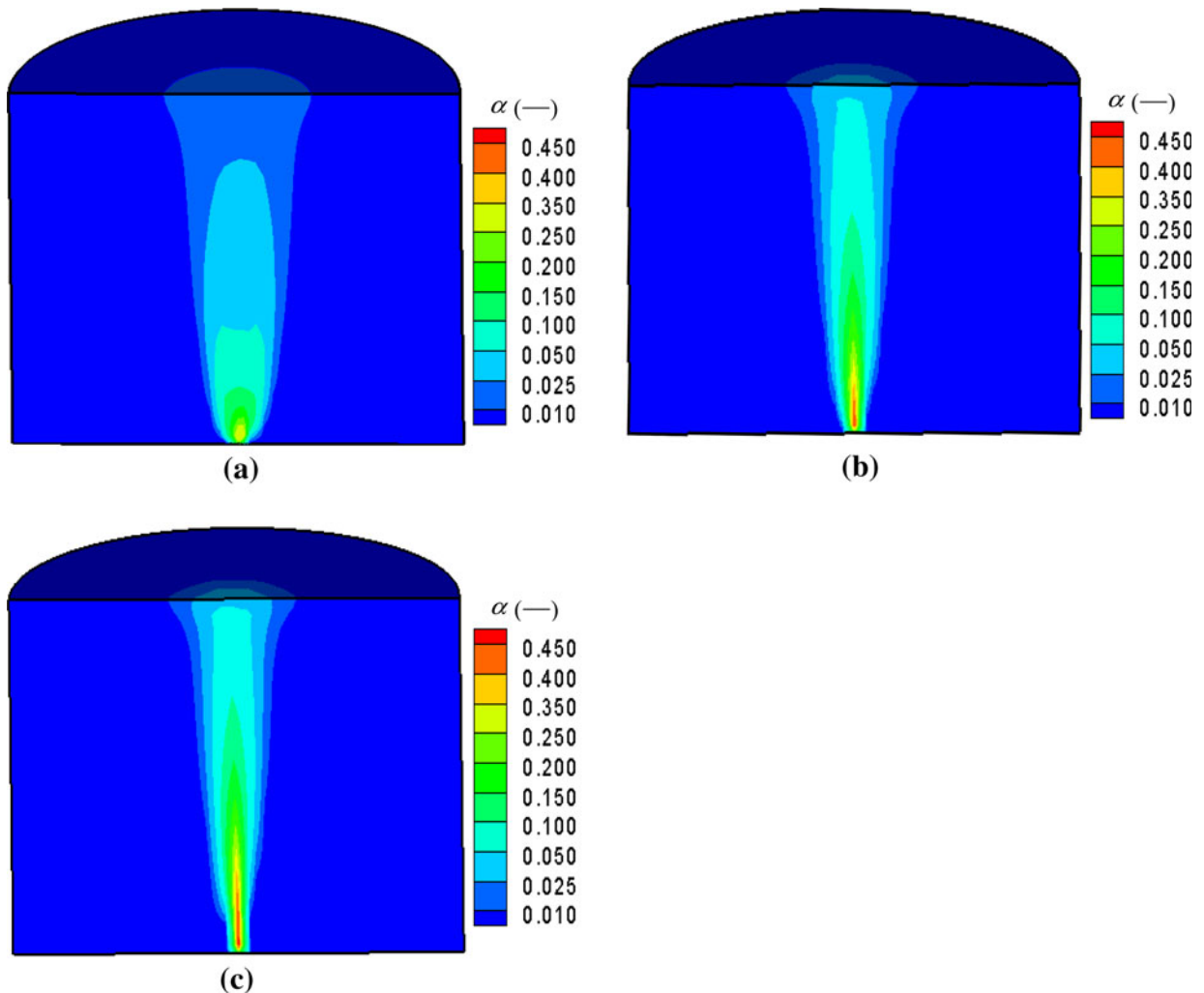

Fig. 9—Effect of different lift coefficient C_L on the predicted contours of gas volume fraction: (*a*) $C_L = 0.5$, (*b*) $C_L = 0$, and (*c*) $C_L = -0.05$.
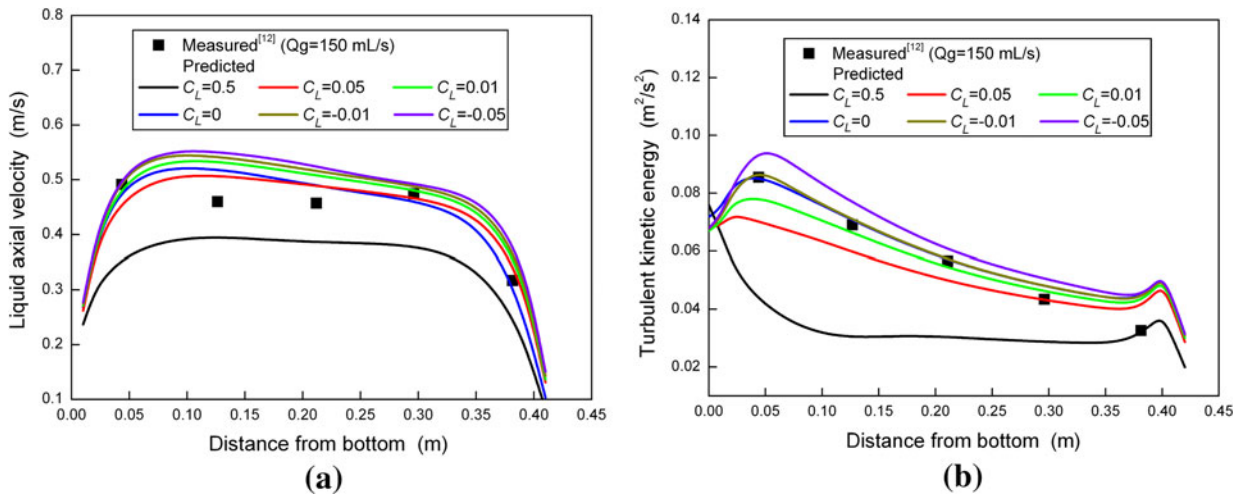
Fig. 10—Comparison between predicted results with different lift force coefficient C_L and measured data from Ref. [12] along the plume centerline: (*a*) axial velocity and (*b*) turbulent kinetic energy.
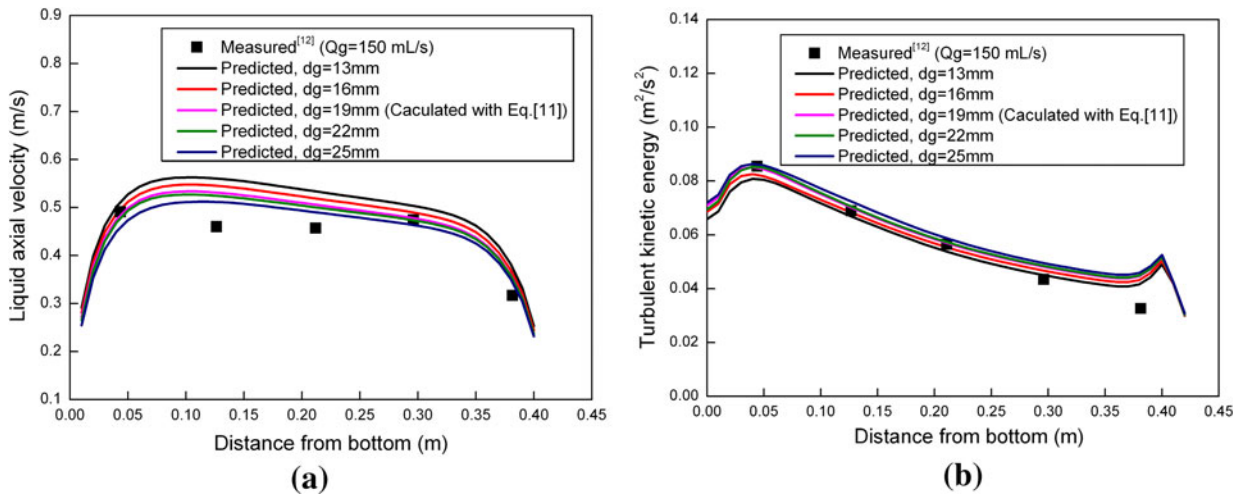

Fig. 11—Effect of bubbles diameter on the predicted (*a*) liquid axial velocity and (*b*) turbulent kinetic energy along the plume centerline.
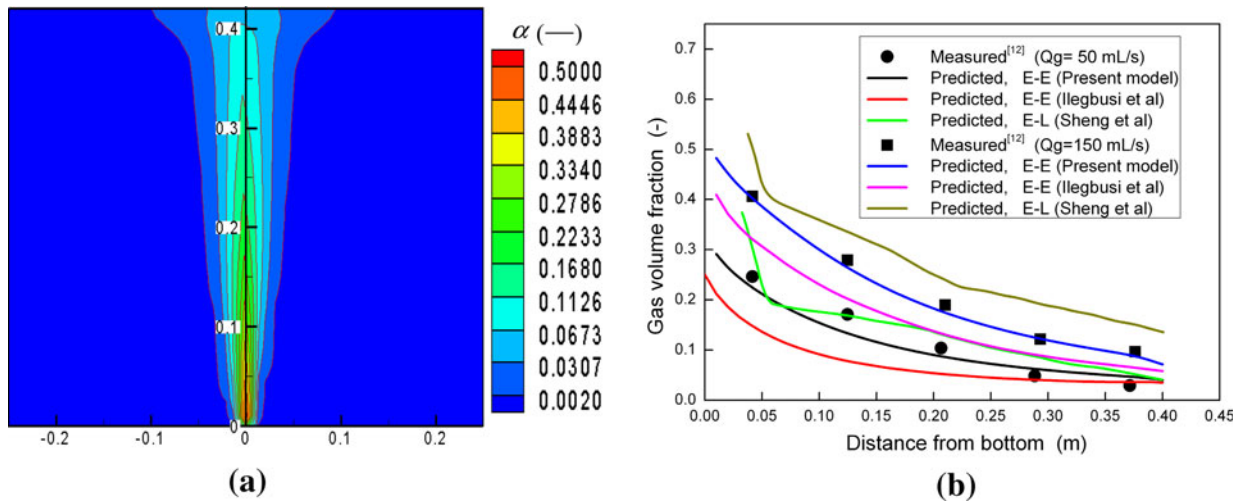

Fig. 12—(*a*) Contour map of gas volume fraction predicted by the current model ($Q_g = 150$ mL/s). (*b*) Comparison of predicted and measured[12] local gas fraction along the plume centerline.

measured data than other models. For the Euler–Lagrange model, the predicted result has a big error under a higher gas flow rate, and the bubble volume fraction was obtained by a statistics of number and residence time of discrete particles in the grid control cell as shown in Eq. [1], which was affected by the grid size and particle number released from the gas inlet. Therefore, the greater the gas flow rate, the greater the error is, and the particle stochastic trajectory would also increase the instability of spatial distribution of the gas volume fraction. For the early Euler–Euler model proposed by Ilegbusi et al.,[18–20] the predicted gas volume fraction along the plume centerline is underpredicted. This may be because that the bubble turbulent diffusion coefficient, which represents liquid turbulent viscosity, is overestimated compared to the current model expression in Eqs. [16] through [24].

Figures 13 and 14 show the comparison of the predicted and measured liquid velocity and turbulent kinetic energy along the centerline of the plume and the radial direction 0.21 m from the bottom, respectively. From these figures, it can be seen that the current model provides the best fit under different gas flow rates. For the early Euler--Euler model, the liquid velocity was underpredicted and the turbulent kinetic energy was overpredicted along the plume centerline. This is because the interphase forces and the bubble-induce turbulent are not accurately quantified in this model. For the Euler–Lagrange model, the predicted velocity agrees well with measured data along the plume centerline; however, the turbulent kinetic energy is still underpredicted, and the predicted liquid velocity is inconsistent with the measured data along the radial direction due to the excessive size of the predicted bubbly plume boundary.
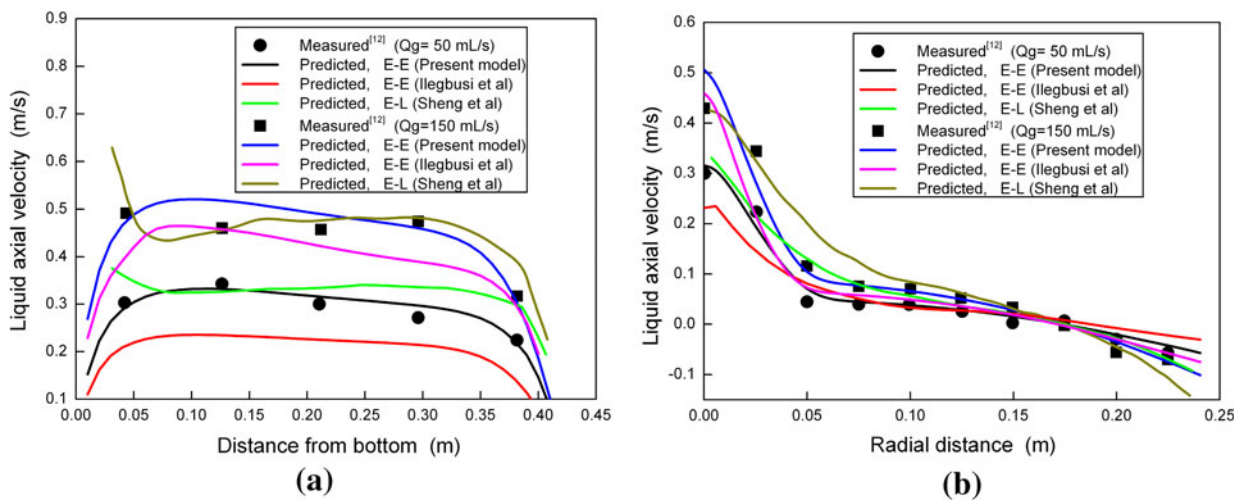

Fig. 13—Comparison between predicted and measured[12] liquid axial velocity along the (a) plume centerline and (b) radial direction 0.21 m from the bottom under a different gas flow rate.
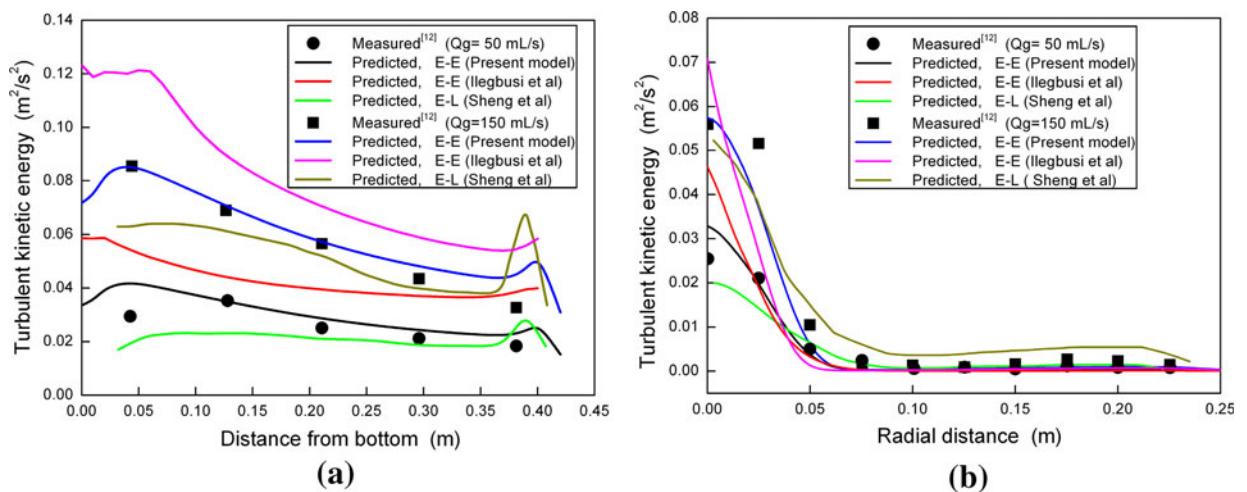

Fig. 14—Comparison between predicted and measured[12] liquid turbulent kinetic energy along (a) the plume centerline and (b) radial direction 0.21 m from the bottom under different gas flow rate.

V. CONCLUSIONS

Based on the Euler–Euler approach, the gas and liquid two-phase flow model was established to describe the gas-stirred system for steelmaking, and the interaction forces between gas-liquid two phases were considered, such as drag force, lift force, and turbulent dispersion force due to liquid velocity fluctuation. The modified k–ε model with extra source terms to account for the bubble-induced turbulence was adopted to model the turbulence in the system. The simulations have been carried out using the Fluent code with user-defined programs. The predicted results were compared with the measured data, and the performances of the current model, the Euler–Lagrange model proposed by Sheng and Irons,[12–14] and the early Euler–Euler model proposed by Ilegbusi et al.[18–20] were assessed. The conclusions are as follows:

1. The bubbly plume produces dispersion due to the liquid velocity fluctuation, and the turbulent dispersion force, which is included in the source term of momentum conservation equation, dominates the bubbly plume shape and is responsible for successful prediction of the gas volume fraction. The current model predictions of bubbly plume shape and local gas volume fraction agree well with the measurement.
2. The bubble-induced turbulence has a significant influence on the liquid velocity and turbulence, and with the turbulent conversion coefficient C_b increasing, the more energy generated during the bubbles rising is converted into liquid turbulence. When the C_b ranged between 0.8 and 0.9, the predicted liquid velocity and turbulent kinetic energy agree well with the measured data.
3. The drag force strongly influences the bubbly plume dynamics and the predicted result agrees well with the measured results as the drag coefficient model proposed by Kolev[38] was adopted. However, the lift force and bubble diameter do not have so much influence on the current bubbly plume system.
4. Under a different gas flow rate, the current Euler–Euler model provides a better fit than the Euler–Lagrange model and the early Euler–Euler approach, and the gas volume fraction distribution and turbulent flow in gas-stirred system are predicted more accurately.

ABBREVIATIONS

NOMENCLATURE

C_A	Virtual mass force coefficient (–)
C_b	Turbulent conversion coefficient (–)
C_D	Drag force coefficient (–)
C_L	Lift force coefficient (–)
D_{gl}^t	Turbulent dispersion coefficient (–)
e_R	Total rate of pressure energy lost by the bubble (kg m^2/s^3)
e_D	Rate of energy converted into turbulence and spent in viscous dissipation (kg m^2/s^3)
Eo	Eötvös number (–) $Eo = g(\rho_l - \rho_g)d_g^2 / \sigma$
F_D	Drag force per unit volume (N/m^3)
F_L	Lift force per unit volume (N/m^3)
F_{VM}	Virtual mass force per unit volume (N/m^3)
F_{TD}	Turbulent dispersion force per unit volume (N/m^3)
$G_{k,l}$	Production of turbulent kinetic energy due to liquid mean velocity gradients (m^2/s^3)
G_b	Bubble-induced turbulent kinetic energy (m^2/s^3)
d_g	Diameter of the bubbles (m)
d_0	Diameter of the nozzle (m)
dt_i	Residence time of the ith bubble in the control cell volume (s)
$\bar{g}$	acceleration due to gravity (m^2/s)
H	Bath liquid height (m)
k_l	Liquid turbulent kinetic energy (m^2/s^2)
$\overline{M}_k$	interphase momentum exchange term (N/m^3)
M_{Wg}	Molecular weight of gas phase (kg/kmol)
N	Number of bubbles particle released from the gas-inlet (–)
P	Static pressure (Pa)
P_{op}	Operating pressure (Pa)
Q_g	Gas flow rate (m^3/s)
R	Universal gas constant (J/(mol K))
Re	Local bubble Reynolds number (–) Re $= \rho_l(u_g - u_l)d_g / \mu_l$
$\bar{u}_l$	liquid velocity (m/s)
$\bar{u}_g$	gas velocity (m/s)
u_{drift}	Ddrift velocity between liquid and gas (m/s)
V	Liquid velocity magnitude (m/s)
V_{cell}	Grid cell volume (m^3)
$V_{bub,pi}$	Volume of the ith bubble in the control cell volume (m^3)
We	Webber number (–) $We = \rho_l(u_l - u_g)^2 d_g / \sigma$
z	Height far from the bath bottom (m)
α	Volume fraction (–)
ρ_l, ρ_g	Liquid and gas density (kg/m^3)
μ_l, μ_t, μ_{eff}	Liquid molecular viscosity, turbulent viscosity, effective viscosity (kg/(m s))
σ	Gas–liquid surface tension coefficient (N/m)
ω_{gl}	Dispersion Prandtl number (–)
τ_{gl}^t	Bubble turbulent characteristic time (s)
τ_{gl}^F	Characteristic time of particle entrainment by the continuous fluid motion (s)
τ_l^t	Characteristic time of the energetic turbulent eddies (s)
θ	Angle between the mean particle velocity and the mean relative velocity (rad)
ε_l	Turbulent dissipation rate (m^2/s^3)

$\Pi_{k,l}$, $\Pi_{\varepsilon,l}$ Influence of the dispersed phases turbulence on the continuous phase turbulence in Eqs. [25] and [26][50,51]

SUBSCRIPT

g   Gas phase
l   Liquid phase

REFERENCES

1. J.S. Joo, J. Szekely, A.H. Castillejos, and J.K. Brimacombe: *Metall. Trans. B*, 1990, vol. 21B, pp. 269–77.
2. D. Mazumdar, R.I.L. Guthrie, and Y. Sahai: *Appl. Math. Model.*, 1993, vol. 17, pp. 255–62.
3. D. Mazumdar and R.I.L. Guthrie: *Metall. Trans. B*, 1985, vol. 16B, pp. 83–90.
4. A.H. Castillejos, M.E. Salcudean, and J.K. Brimacombe: *Metall. Trans. B*, 1989, vol. 20B, pp. 603–11.
5. J.S. Joo and R.I.L. Guthrie: *Metall. Trans. B*, 1992, vol. 23B, pp. 765–78.
6. M.Y. Zhu, T. Inomoto, I. Sawada, and T.C. Hsiao: *ISIJ Int.*, 1995, vol. 35, pp. 472–79.
7. M.Y. Zhu, I. Sawada, N. Yamasaki, and T.C. Hsiao: *ISIJ Int.*, 1996, vol. 36, pp. 503–11.
8. J.H. Grevet, J. Szekely, and N. El Kaddah: *Int. J. Heat Mass Trans.*, 1982, vol. 25, pp. 487–97.
9. Y. Sahai and R.I.L. Guthrie: *Metall. Trans. B*, 1982, vol. 13B, pp. 203–11.
10. A.H. Castillejos, M. Salcudean, and J.K. Brimacombe: *Metall. Trans. B*, 1989, vol. 20B, pp. 603–11.
11. S.T. Johansen and F. Boysan: *Metall. Trans. B*, 1988, vol. 19B, pp. 755–64.
12. Y. Sheng and G. Irons: *Metall. Trans. B*, 1993, vol. 24B, pp. 695–705.
13. Y. Sheng and G. Irons: *Metall. Mater. Trans. B*, 1995, vol. 26B, pp. 625–35.
14. D. Guo and G. Irons: *Metall. Mater. Trans. B*, 2000, vol. 31B, pp. 1457–64.
15. D. Mazumdar and R.I.L. Guthrie: *ISIJ Int.*, 1994, vol. 34, pp. 384–92.
16. H. Turkoglu and B. Farouk: *ISIJ Int.*, 1991, vol. 31, pp. 1371–80.
17. H. Turkoglu and B. Farouk: *Metall. Trans. B*, 1990, vol. 21B, pp. 771–81.
18. O.J. Ilegbusi and J. Szekely: *ISIJ Int.*, 1990, vol. 30, pp. 731–39.
19. O.J. Ilegbusi, J. Szekely, M. Iguchi, H. Takeuchi, and Z. Morita: *ISIJ Int.*, 1993, vol. 33, pp. 474–78.
20. O.J. Ilegbusi, M. Iguchi, K. Nakajima, M. Sano, and M. Sakamoto: *Metall. Mater. Trans. B*, 1998, vol. 29B, pp. 211–22.
21. G. Venturini and M.B. Goladschmit: *Metall. Mater. Trans. B*, 2007, vol. 38B, pp. 461–75.
22. D.Y. Sheng, M. Söder, P. Jönsson, and L. Jonsson: *Scand. J. Metall.*, 2002, vol. 31, pp. 134–47.
23. T. Qu, M. Jiang, C. Liu, and Y. Komizo: *Steel Res. Int.*, 2010, vol. 81, pp. 434–45.
24. Fluent Inc.: *FLUENT 6.3 User's Guide*, Fluent Inc., Lebanon, NH, 2006.
25. P.J. Smith, F. Thomas, and L.D. Smoot: *Eighteenth Symposium (International) on Combustion*, vol. 18, 1981, pp. 1285–93.
26. A.S. Abbas, S.S. Koussa, and F.C. Lockwood: *Eighteenth Symposium (International) on Combustion*, vol. 18, 1981, pp. 1427–38.
27. O. Simonin: *Fifth Workshop on Two-Phase Flow Predictions, Proc. LSTM*, Erlangen, Germany, 1990, pp. 156-66.
28. O. Simonin and P.L. Viollet: *Numerical Methods for Multiphase Flows, FED*, vol. 91, ASM International, Materials Park, OH, 1990, pp. 65–82.
29. O. Simonin, E. Deutsch, and J.P. Minier: *Appl. Sci. Res.*, 1993, vol. 51, pp. 275–83.
30. N. Huda, J. Naser, G. Brooks, M.A. Reuter, and R. Matusewicz: *Metall. Mater. Trans. B*, 2010, vol. 41B, pp. 35–50.
31. N. Huda, J. Naser, G. Brooks, M.A. Reuter, and R. Matusewicz: *Metall. Mater. Trans. B*, 2012, vol. 43B, pp. 39–55.
32. R.F. Mudde and O. Simonin: *Chem. Eng. Sci.*, 1999, vol. 54, pp. 5061–69.
33. E. Delnoij, J.A.M. Kuipers, and W.P.M. van Swaaij: *Chem. Eng. Sci.*, 1997, vol. 52, pp. 1429–58.
34. R. Djebbar, M. Roustan, and A. Line: *Trans. IChemE*, 1996, vol. 74, pp. 492–98.
35. A. Tomiyama, I. Kataoka, and I. Zunb: *JSME Int. J. Ser. B*, 1998, vol. 41, pp. 472–79.
36. A. Tomiyama, H. Tamaia, and I. Zunb: *Chem. Eng. Sci.*, 2002, vol. 57, pp. 1849–58.
37. M. Ishii and N. Zuber: *A.I.Ch.E. J.*, 1979, vol. 25, pp. 843–55.
38. J.T. Kuo and G.B. Wallis: *Int. J. Multiphas. Flow*, 1988, vol. 14, pp. 547–64.
39. N. Boisson and M.R. Malin: *Int. J. Numer. Methods Fluid*, 1996, vol. 23, pp. 1289–310.
40. N.I. Kolev: *Multiphase Flow Dynamics 2: Thermal and Mechanical Interactions*, 2nd ed., Springer, Berlin, Germany, 2005.
41. K. Kuwagi and H. Ozoe: *Int. J. Multiph. Flow*, 1999, vol. 25, pp. 175–82.
42. Y. Murai and Y. Matsumoto: *JSME Int. J. Ser. B*, 1998. vol. 41, pp. 568–74.
43. M. Lopez de Bertodano, R.T. Lahey, Jr., and O.C. Jones: *Int. J. Multiph. Flow*, 1994, vol. 20, pp. 805–18.
44. A. Tomiyama: *Proceeding of the Third International Conference on Multiphase Flow*, Lyon, France, 1998.
45. J. Grienberger and H. Hofmann: *Chem. Eng. Sci.*, 1992, vol. 47, pp. 2215–20.
46. H.F. Svendsen, H.A. Jakobsen, and R. Torvik: *Chem. Eng. Sci.*, 1992, vol. 47, pp. 3297–304.
47. D. Pfleger and S. Becker: *Chem. Eng. Sci.*, 2001, vol. 56, pp. 1737–47.
48. B.M. Lopez, R.T. Lahey, and O.C. Jones: *J. Fluid Eng.*, 1994, vol. 116, pp. 128–34.
49. M. Sano and K. Mori: *Trans. Jpn. Inst. Met.*, 1976, vol. 17, pp. 344–52.
50. D. Zhang, N.G. Deen, and J.A.M. Kuipers: *Chem. Eng. Sci.*, 2006, vol. 61, pp. 7593–608.
51. J.B. Joshi: *Chem. Eng. Sci.*, 2001, vol. 56, pp. 5893–933.
52. M. Lopez de Bertodano, S.J. Lee, and R.T. Lahey, Jr.: *J. Fluid Eng.*, 1990, vol. 112, pp. 107–13.
53. R. Bel F'Dhila and O. Simonin: *Sixth Workshop on Two-Phase Flow Predictions*, Erlangen, Germany, 1992.
54. S. Elgobashi and T. Abou-Arab: *Phys. Fluid.*, 1983, vol. 26, pp. 931–38.
55. A.H. Castillejos and J.K. Brimacombe: *Metall. Trans. B*, 1987, vol. 18B, pp. 659–71.